NeuroImage 253 (2022) 119050

Contents lists available at ScienceDirect

NeuroImage

journal homepage: www.elsevier.com/locate/neuroimage

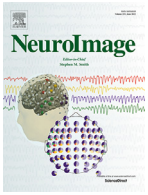

Non-invasive recording of high-frequency signals from the human spinal cord

Bankim Subhash Chander[a,b,1,2], Matthias Deliano[c,1], Elena Azañón[a,b,d], Lars Büntjen[e], Max-Philipp Stenner[a,b,d,*]

[a] Department of Neurology, Otto-von-Guericke University, Magdeburg, Germany
[b] Department of Behavioral Neurology, Leibniz Institute for Neurobiology, Magdeburg, Germany
[c] Combinatorial NeuroImaging Core Facility, Leibniz Institute for Neurobiology, Magdeburg, Germany
[d] Center for Behavioral Brain Sciences, Magdeburg, Germany
[e] Department of Stereotactic Neurosurgery, Otto-von-Guericke University, Magdeburg, Germany

ARTICLE INFO

Keywords:
Somatosensory system
Spinal cord
Spike-like potentials
High-frequency oscillations
Median nerve stimulation
Electroencephalography

ABSTRACT

Throughout the somatosensory system, neuronal ensembles generate high-frequency signals in the range of several hundred Hertz in response to sensory input. High-frequency signals have been related to neuronal spiking, and could thus help clarify the functional architecture of sensory processing. Recording high-frequency signals from subcortical regions, however, has been limited to clinical pathology whose treatment allows for invasive recordings. Here, we demonstrate the feasibility to record 200–1200 Hz signals from the human spinal cord non-invasively, and in healthy individuals. Using standard electroencephalography equipment in a cervical electrode montage, we observed high-frequency signals between 200 and 1200 Hz in a time window between 8 and 16 ms after electric median nerve stimulation (n = 15). These signals overlapped in latency, and, partly, in frequency, with signals obtained via invasive, epidural recordings from the spinal cord in a patient with neuropathic pain. Importantly, the observed high-frequency signals were dissociable from classic spinal evoked responses. A spatial filter that optimized the signal-to-noise ratio of high-frequency signals led to submaximal amplitudes of the evoked response, and vice versa, ruling out the possibility that high-frequency signals are merely a spectral representation of the evoked response. Furthermore, we observed spontaneous fluctuations in the amplitude of high-frequency signals over time, in the absence of any concurrent, systematic change to the evoked response. High-frequency, "spike-like" signals from the human spinal cord thus carry information that is complementary to the evoked response. The possibility to assess these signals non-invasively provides a novel window onto the neurophysiology of the human spinal cord, both in a context of top-down control over perception, as well as in pathology.

1. Introduction

Spatially and temporally resolved recordings of neuronal activity are an important tool in neuroscience. To study neurophysiology in healthy humans, such recordings have to be non-invasive. Electro- and magnetoencephalography (EEG, MEG) are non-invasive techniques that provide high temporal resolution, in principle high enough to detect neuronal population signals up to several kHz. Yet a major focus in MEG and EEG research has been on signals in the range of classic EEG frequency bands, i.e., below approximately 100 Hz. Signals below ~100 Hz are thought to reflect a population measure of synaptic input (as well as spike after-potentials and membrane potential oscillations; Logothetis, 2003).

However, neuronal ensembles generate signals that can be of much higher frequency, i.e., above 400 Hz (Buzsáki et al., 2004), and even around 1 kHz (Fedele et al., 2015). Input to the somatosensory system, for example, induces high-frequency oscillations (HFO) at around 600 Hz overlying the N20 evoked potential in scalp EEG and in MEG

Abbreviations: HFO, High frequency oscillations; EEG, Electroencephalography; MEG, Magnetoencephalography; SEP, somatosensory evoked potentials; DBS, Deep brain stimulation; LFP, Local field potentials; SCS, Spinal cord stimulation; ERP, Event-related potential; DSS, Denoising separation of sources.

* Corresponding author at: Department of Neurology, Otto-von-Guericke University, Leipziger Str. 44, Magdeburg 39120, Germany
E-mail address: max-philipp.stenner@med.ovgu.de (M.-P. Stenner).

[1] These authors contributed equally to this work.

[2] Present address: Department of Psychiatry and Psychotherapy, Center for Innovative Psychiatric and Psychotherapeutic Research, Central Institute of Mental Health Mannheim, Medical Faculty Mannheim, University of Heidelberg, Mannheim, Germany.

https://doi.org/10.1016/j.neuroimage.2022.119050.
Received 25 August 2021; Received in revised form 16 February 2022; Accepted 1 March 2022
Available online 8 March 2022.

(Cracco and Cracco, 1976; Yamada et al., 1988; Curio et al., 1994; Hashimoto et al., 1999; for a review, see Ozaki and Hashimoto, 2011). Signal frequencies above 400 Hz, or even around 1 kHz, approach time scales of action potentials, i.e., neuronal signals whose information content is fundamentally different from synaptic input. Indeed, HFO around 600 Hz correlate with neuronal spiking (Baker et al., 2003; Telenczuk et al., 2011), leading some authors to label them as "spike-like" (Gobbelé et al., 1999; Klostermann et al., 2001a, 2001b; Fedele et al., 2015). HFO may thus carry unique information that is complementary to classic EEG frequency bands below 100 Hz (Logothetis, 2003). For example, low-frequency signals may not dissociate between excitation and inhibition (e.g., Peterson et al., 1995; Wikström et al., 1996), and between sub- and supra-threshold (mass) synaptic input, while (a population measure of) neuronal spiking could (Telenczuk and Destexhe, 2014; Herreras, 2016).

However, MEG and EEG research into human perception (e.g., Arnal and Giraud, 2012), action (e.g., van Wijk et al., 2012), and cognition (e.g., Ward, 2003) has focused on classic EEG frequency bands, i.e., signals below approximately 100 Hz, while the role of high-frequency population signals above 400 Hz in these systems-level brain functions has remained largely unknown. For example, it is largely unknown whether, and in which regions of the nervous system, modulatory effects of attention or expectation involve HFO. This is surprising, given that their relation to neuronal spiking (Baker et al., 2003; Telenczuk et al., 2011) could, in principle, help understand the functional architecture of modulatory factors such as attention or expectation, beyond information provided by lower-frequency signals.

Indeed, others have considered a possible involvement of HFO in modulatory effects of attention before. Klostermann et al. (2001b) observed that the amplitude of HFO in scalp EEG fluctuates more strongly over time than the amplitude of the N20 evoked response, fluctuations which, the authors proposed, may reflect a floating focus of attention (but see Gobbelé et al., 2000). Other studies have provided further evidence for a functional dissociation between HFO in scalp EEG and somatosensory evoked potentials. For example, the N20 somatosensory evoked potential and somatosensory induced HFO show differential modulation by sleep (Hashimoto et al., 1996), hyperventilation (Mochizuki et al., 2003), and tactile interference stimulation (Hashimoto et al., 1999). While these studies point to specific cell types that may generate HFO (Hashimoto et al., 1996, 1999; Ozaki and Hashimoto, 2011), they reveal relatively little about the role of these signals in bottom-up and/or top-down information flow for perception.

A dissociation between HFO and evoked responses exists also for subcortical signals. HFO are elicited by electric stimulation of the median nerve in the hand area in somatosensory cortex (Curio et al., 1994, 1997; Baker et al., 2003), but are also found in invasive recordings from thalamus (Klostermann et al., 1999a), brainstem (Restuccia et al., 2004), and in epidural recordings from the human spinal cord (Insola et al., 2008). Similar to their respective counterparts in scalp EEG, thalamic HFO vary over time independently from thalamic evoked responses (Klostermann et al., 1999a). Even at pre-thalamic stages of somatosensory processing, HFO are modulated systematically, and independently of longer-latency HFO in scalp EEG. Recording from nasopharyngeal electrodes, i.e., in the vicinity of the medulla oblongata, for example, show an increase in the amplitude of HFO when opening the eyes, while cortical HFO remain unchanged (Restuccia et al., 2004; but see Gobbelé et al., 2000).

The earliest possible stage of somatosensory processing in the central nervous system is the spinal cord. Previous functional imaging studies suggest that the spinal cord may pre-process nociceptive input as a function of attention (Sprenger et al., 2012) and expectation (Eippert et al., 2009). A particularly early mechanism of gating input to the central nervous system is a pre-synaptic modulation of afferent drive to the spinal cord, e.g., during movement (Seki et al., 2003). Such pre-synaptic gating mechanisms may contribute to symptom generation in movement disorders (Lira et al., 2020) and to pain control (Melzack and Wall, 1965; Guo and Hu, 2014). Given that HFO may represent a population signal of neuronal spiking (Baker et al., 2003; Telenczuk et al., 2011), i.e., pre-synaptic processes, studying spinal HFO has the potential to reveal physiological, pathophysiological, and therapeutically relevant principles of early somatosensory processing in the central nervous system.

To date, however, spinal HFO have received little attention. An important reason for this is that recordings of spinal HFO have been exclusively invasive. Insola et al. (2008) have demonstrated HFO at the level of the human spinal cord, recorded via epidural electrodes implanted for pain relief (pain relief is achieved via electric stimulation). Moreover, Insola et al. (2008) observed a decrease in the amplitude of HFO (at ~1200 Hz) during wrist movements. This underscores the idea that somatosensory input is pre-processed as early as at the level of the spinal cord, and that such pre-processing involves HFO. However, Insola et al's. (2008) invasive recordings also illustrate that data in support of this idea have only been available in a clinical, post-surgical context to which such invasive recordings have been limited, to date. Can HFO be recorded non-invasively from the human spinal cord, in the absence of pathology, medication, and recent surgery?

Here, we demonstrate that HFO between 200 and 1200 Hz, which are detectable in invasive, epidural recordings in a patient with pain, can also be recorded non-invasively from healthy humans, using standard electroencephalography equipment and an established, cervical electrode montage (Restuccia and Mauguière, 1991). We show that these spinal HFO are dissociable from classic spinal evoked responses. Specifically, a spatial filter that maximizes the evoked response does not fully capture the observed high-frequency signals, and vice versa. Furthermore, the amplitude of high-frequency signals spontaneously fluctuates over time in the absence of any systematic change to the evoked response. Spinal HFO therefore carry information that is complementary to spinal evoked responses. Non-invasive recordings of spinal HFO thus provide a novel window onto the neurophysiology of the human spinal cord.

2. Materials and methods

2.1. Subjects

We recruited 17 healthy volunteers (nine men, eight women; age range 18–37 years, mean 27.5 years) for the non-invasive recording of spinal potentials from the skin surface of the neck. Two participants were excluded because median nerve stimulation did not result in a reliable thumb twitch throughout the recording session, so that stability of stimulation across the recording session could not be monitored. In addition, we recorded local field potentials (LFP) via an epidural electrode placed alongside the dorsal spinal cord, spanning vertebra levels four to six (Boston Scientific Linear SC-2218–70), in a 40-year-old female patient with neuropathic pain due to complex regional pain syndrome of the right hand. At the time of the recording, the patient was medicated with 50 mg Amitriptyline, 60 mg Duloxetine, 300 mg Pregabalin, and 20/10 mg Oxycodone. Recordings were conducted on the third day after surgery, when leads were still externalised as part of the standard medical procedure. All participants gave written informed consent. The study was approved by the local ethics committee, and conducted in accordance with the Declaration of Helsinki.

2.2. Median nerve stimulation & experimental task

Experiments were conducted in a dimly lit, electrically shielded, and sound-attenuated chamber (Industrial Acoustics Company GmbH). The left median nerve was electrically stimulated via surface electrodes at the wrist (Ambu Neuroline 700) using a DS7 stimulator (Digitimer Ltd.). The stimulator delivered a constant current square wave pulse (proximal electrode positive) at a stimulus intensity above motor threshold. Motor threshold was determined as the stimulator's output voltage that

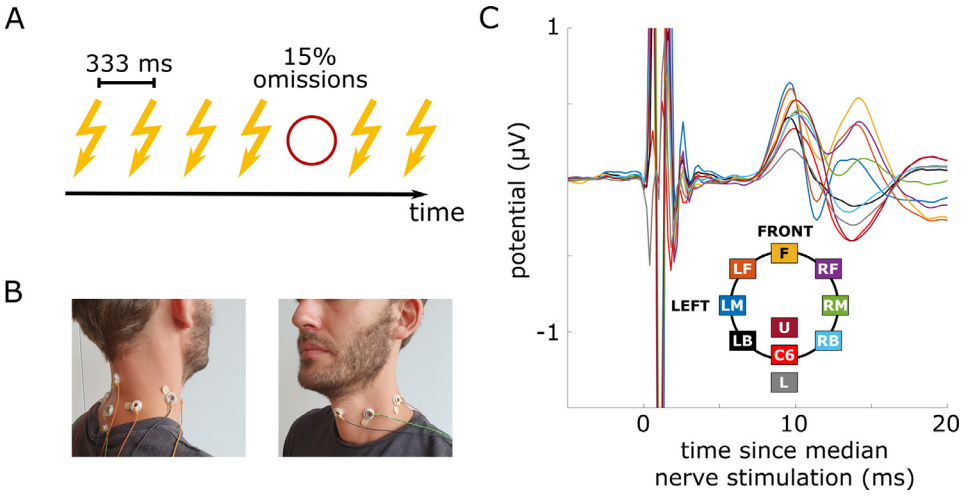

Fig. 1. *Experimental task, electrode montage, and grand-average evoked response across channels for healthy volunteers*. Flashes in ***A*** represent electric median nerve stimulation. The red circle represents an omission of stimulation. In ***B*** *(electrode montage)*, reference and ground electrodes (placed onto right and left acromion, respectively) are not shown, nor are scalp electrodes. Colors used for time-courses in ***C*** *(grand-average evoked response)* code for channels, as shown in the inset: *C6* (spinous process of C6); *LB*, left back; *LM*, left middle; *LF*, left front; *F*, front; *RF*, right front; *RM*, right middle; *RB*, right back; *U*, 5 cm cranial of C6; *L*, 3 cm caudal of C6.

elicited a visible thumb twitch at least 5 out of 10 times. Stimulation intensity was set to 110% of the individually determined motor threshold (mean 75 mA, range 25–100 mA). The elicited thumb twitch allowed us to monitor stability of stimulation across the recording session. Stimulation pulse width was set to 50 μs (two healthy participants, as well as for the patient), 200 μs (four participants), or 500 μs (10 participants), depending on which pulse width was sufficient for eliciting a thumb twitch below the maximum output voltage of the stimulator. We excluded two participants from analysis because they did not show any visible thumb twitch, or only an inconsistent/rare thumb twitch, even at the maximum tolerable median nerve stimulation intensity, likely due to suboptimal placement of stimulation electrodes.

We applied median nerve stimulation at a frequency of 3 Hz (2 Hz in the patient). 15% of stimuli were pseudo-randomly omitted (**Fig. 1A**), such that there were no consecutive omissions, and the median nerve was always stimulated in the first and last trial in each block of one minute. Our motivation to include unexpected omissions was twofold. First, we wanted to add task-relevance to the median nerve stimulation by asking participants to count, silently, the number of omissions. Stimulation was stopped after 60 s and participants reported the number of omissions in the preceding minute. Second, we wanted to test for omission responses at latencies that would indicate a spinal locus. Because we found no evidence of an evoked or induced response to an omission at a latency that would indicate a spinal locus (<~15 ms after median nerve stimulation), omission trials are not considered further throughout the manuscript.

Healthy volunteers completed between 57 and 109 one-minute blocks (mean 82.9, SD 14.6; the session was terminated once a volunteer reported fatigue), while the patient completed 34 one-minute blocks.

2.3. Montage and recording of spinal potentials

Eight standard EEG electrodes were placed in a ring formation around the neck (**Fig. 1B** and **C**), using an established, cervical electrode montage (Restuccia and Mauguière, 1991), with the electrode at the back of the neck above the spinous process of the sixth cervical vertebra, and the electrode at the front placed onto the thyroid cartilage. The remaining six electrodes were evenly spaced around the neck between front and back, both on the left and right side, in a transverse plane defined by the spinous process of the sixth cervical vertebra (Restuccia and Mauguière, 1991). Additionally, two more electrodes were attached 5 cm above and 3 cm below the sixth cervical spinous process electrode. The reference electrode was placed over the right acromion, and the ground electrode was placed over the left acromion. Electrodes were attached to the skin using electrode holders and double adhesive electrode washers. The void between the electrode and the skin was filled with a conductive abrasive gel, and the impedance of the electrodes was maintained below 5 kOhms. Non-invasive spinal recordings were digitized at a sampling frequency of 5000 Hz using a 32 channels BrainAmp DC apparatus (Brain Products GmbH). The hardware highpass filter was set to 0.1 s to avoid low frequency drifts, and a hardware anti-aliasing low pass filter was set to 1000 Hz (30 dB/octave roll-off). Simultaneous to cervical recordings, and via the same amplifier, we recorded scalp EEG from a total of 9–13 channels, as well as the electrooculogram and an ECG (not reported).

In the patient receiving spinal cord stimulation (SCS) for the treatment of neuropathic pain, epidural LFP were recorded via an implanted SCS-electrode with eight contacts (**Fig. 6A, left**). The fourth contact from the top was used as a reference. LFP recordings were grounded to a wire wrapped around the cables connecting electrode contacts to our recording system. Invasive recordings were digitized at a sampling frequency of 2500 Hz, with the same online filter settings as described above. SCS was turned off during recording.

2.4. EEG analysis

2.4.1. ECG removal, epoching, and trial rejection

EEG analysis used FieldTrip (Oostenveld et al., 2011), NoiseTools (De Cheveigne and Parra, 2014; http://audition.ens.fr/adc/NoiseTools/), and custom-written scripts in Matlab. For data from both non-invasive and invasive recordings, we first removed ECG artefacts using template subtraction. We identified R peaks after band pass filtering data from the ECG electrode between 3 and 25 Hz (no spectral filter was applied to any of the other channels). The first R peak was marked manually. Subsequent R peaks were identified via a threshold to correlation coefficients derived from a correlation with a moving average across the last ten PQRST complexes detected so far. For each PQRST complex, the mean across the preceding and subsequent five PQRST complexes, from −600 to +600 ms around each R peak, was subtracted after filtering with a Hanning taper to avoid edge artefacts.

Data were epoched from −350 ms to 350 ms relative to each median nerve stimulus. Epochs from non-invasive recordings were demeaned and de-trended (linear trend). We rejected epochs based on three criteria. These were the maximum absolute z-value across time (cut-off: 10), the mean absolute z-value across time (cut-off: 3), and the variance across time (cut-off: 5 standard deviations above the mean across epochs; for all three parameters, we focused on a time window between −150 and +50 ms around median nerve stimulation). All three parameters for trial exclusion correspond to standard parameters for trial exclusion used in FieldTrip. Cut-off values were chosen after visual inspection of the three abovementioned parameters for each individual, such that cut-offs reliably isolated clearly visible outliers across individuals.

Based on these exclusion criteria, between 0.45 and 6.9% of trials were excluded (mean: 1.3%, SD: 1.6%). Between 8583 and 16,698 trials were available for analysis (mean: 12,541 trials, SD: 2225 trials).

2.4.2. Spatial filtering

Data from non-invasive recordings were analysed both in the original montage, i.e., without re-referencing (Fig. 2), and following spatial filtering, a procedure recommended for efficient analysis of high-frequency signals in non-invasive cortical recordings (Waterstraat et al., 2015). Denoising Separation of Sources (DSS; also called Joint Decorrelation; De Cheveigne and Parra, 2014) was used to construct a spatial filter that optimized the signal-to-noise ratio of short-latency, high-frequency signals (400–1200 Hz, 8 to 16 ms). DSS jointly diagonalizes the covariance matrix of the original data (C0), and the covariance matrix after applying a "bias filter" that emphasizes the signal of interest (C1). In general, such bias filtering can involve spectral filtering, selection of a time window of interest, and/or averaging across trials (De Cheveigne and Parra, 2014).

Given our *a priori* hypothesis about the approximate frequency band (400–1200 Hz) and time window (8 to 16 ms) of spinal high-frequency signals (Insola et al., 2008), we combined spectral filtering with a "bias filter" that emphasized our time window of interest to construct spatial filters optimized for spinal high-frequency signals. Specifically, we band-pass filtered continuous data between 400 and 1200 Hz (4th order Butterworth filter) after ECG removal (see above). Importantly, we used band-pass filtering only to construct spatial filters, while the data subsequently projected through these filters were not band-pass filtered, and thus uncontaminated by potential filter artefacts, and without temporal uncertainties due to convolution in the time-domain. To construct spatial filters, band-pass filtered data were epoched, omitting previously rejected epochs (see above). Epoching was followed by trial- and channel-wise z-transformation (subtraction of the mean amplitude and division by its standard deviation, both computed across time for each trial and channel separately). Z-transformation was included to allow for construction of spatial filters at the group level. We chose group-level over subject-wise construction of spatial filters for three reasons. First, we expected estimation of covariance matrices to profit from the large number (190,550) of trials available across subjects. Second, spatial topographies of spinal signals were expected to be sufficiently similar across individuals to allow for construction of a group-level spatial filter. Third, and most importantly, we wanted to minimize the risk of amplifying noise via spatial filters, a risk we considered higher at a single-subject level.

Z-transformed epochs were concatenated across individuals. Covariance matrix C0 was computed across a large time window from 8 to 200 ms after median nerve stimulation. Covariance matrix C1, on the other hand, was derived from our time window of interest, i.e., 8 to 16 ms after median nerve stimulation, i.e., a time window indicative of signals at the level of the spinal cord (Fig. 1C). With these covariance matrices as input, DSS (nt_dss0.m) provides a spatial filter that optimizes the power-ratio score comparing signals between 400 and 1200 Hz in our time window of interest, and signals between 400 and 1200 Hz across a much larger, 8–200 ms time window (c.f Waterstraat et al., 2015., for a similar logic underlying spatial filtering of scalp-level HFO). DSS filter coefficients were rescaled such that filter coefficients for each component summed to 1. As a result, units are unchanged, and signal amplitudes after projecting through different filters (see Section 2.4.5) are comparable.

To ensure that spatial filtering did not simply amplify noise, we conducted a resampling test. To this end, we re-computed C1 after shifting the 8 ms duration time window for which C1 was computed randomly within an interval between 16 and 200 ms after median nerve stimulation, separately for each trial. Such random shifts of the time axis follow from a null hypothesis assuming purely noise in the time window between 8 and 16 ms after median nerve stimulation. Given this null hypothesis, any other time window should yield a similar power-ratio score after filtering. C1 was thus re-computed 1000 times (each time shifting the time axis of individual trials anew) to obtain a distribution of power-ratio scores under this null hypothesis. We then compared the "true" power-ratio score, computed for a consistent time window between 8 and 16 ms after median nerve stimulation, with this distribution under the null hypothesis. We obtained a p-value for each DSS component as the proportion of resampling iterations with a power-ratio score that exceeded that component's actual, "true" power-ratio score.

To estimate topographies for DSS components, we calculated how strongly data projected through the DSS filter (Fig. 3 A and B) correlated with the original data, i.e., with data before projecting through the DSS filter. This yielded one (Pearson's) correlation coefficient per channel, trial, and component. Correlation coefficients were Fisher z-transformed (atanh.m), averaged across trials, transformed back (tanh.m) and plotted. The resulting spatial distribution of averaged correlation coefficients indicates how similar data at each channel is to a given DSS component. De Cheveigne and Parra (2014) refer to this distribution as a spatial pattern. More generally, a spatial pattern has been defined as the inverse of a spatial filter matrix (Haufe et al., 2014), such as the DSS filter. We therefore compared spatial topographies obtained with the correlation approach described above and spatial topographies that resulted from taking the inverse.

2.4.3. Pre-processing of data from invasive recordings

In the patient, the precise placement of the epidural electrode depended purely on medical considerations. We therefore had no *a priori* hypothesis which of the seven channels would be most responsive to median nerve stimulation. Instead, we computed a single channel offline by subtracting data obtained in the most caudal channel from data obtained in the most cranial channel. The rationale was that any spinal response to median nerve stimulation along the extent of the electrode would be captured by this channel. 3436 trials were available for analysis after rejecting epochs (same criteria as described above; 0.1% of trials excluded).

2.4.4. Time-frequency analysis

Time-frequency analysis was performed in FieldTrip, using FieldTrip's multitaper method (mtmconvol) and a frequency-dependent Hanning taper (5 cycles). Power was computed trial-wise across frequencies ranging from 200 to 1200 Hz in steps of 50 Hz, and at time samples separated by 0.2 ms (corresponding to the sampling frequency), and then averaged across trials. In separate analyses, we minimized signals phase-locked to median nerve stimulation by subtracting the mean, across trials, of the complex-valued Fourier spectra from single-trial Fourier spectra before computing power as the square of the magnitude of the Fourier spectra (Bauer et al., 2012). To examine the spectro-temporal pattern of the evoked response, we conducted time-frequency analyses after averaging across trials. In all time-frequency analyses, baseline power was defined as mean power across a time window from −100 to −20 ms relative to median nerve stimulation, computed for each frequency bin and channel separately. For visualization, time-frequency representations were spectrally interpolated and displayed using Moreland's "cool/warm" color map (Moreland, 2009).

2.4.5. Dissociation of HFO power and evoked response amplitude via spatial filters

To examine whether the power of high-frequency signals is dissociable from the amplitude of the spinal evoked response, and thus rule out the possibility that high-frequency signals are merely a spectral representation of the evoked response, we constructed a second DSS filter, optimized for the evoked response. The goal was to investigate whether a spatial filter optimized for the evoked response would be suboptimal for detecting HFO, compared to the spatial filter constructed for HFO, and vice versa. This would provide evidence that high-frequency signals are not purely a spectral representation of classic spinal evoked responses.

Construction of a DSS filter optimized for the evoked response followed similar steps as described above for spatial filtering of HFO (Section 2.4.2), with two differences. First, data were not band-pass filtered. Second, C1 was computed across the same time window as for HFO (8 to 16 ms), but *after* averaging across epochs, while C0 was computed for a time window between 8 and 200 ms, and across individual trials. In this way, DSS provides a spatial filter that emphasizes signals between 8 and 16 ms, over and above signals in a broader time window up to 200 ms, specifically signals between 8 and 16 ms that are consistent (reproducible) across trials, as expected for the evoked response (Fig. 1C; De Cheveigne and Parra, 2014). A similar resampling test was conducted as described in Section 2.4.2 to ensure that spatial filtering did not simply amplify noise.

We then projected pre-processed data through the DSS filter optimized for HFO, and separately through the DSS filter optimized for the evoked response. To baseline-correct individual-subject evoked responses, we used a time window between −10 and −1 ms relative to median nerve stimulation. We then compared the evoked response obtained after spatial filtering optimized for the evoked response with the evoked response obtained after spatial filtering optimized for HFO. This was done using a cluster-based permutation test (see Section 2.5), and by subjecting single-subject peak amplitudes to a *t*-test (significance level at $p < .05$). For the latter, single-subject peak latencies were identified visually. A cluster-based permutation test was used to compare time-frequency power obtained after spatial filtering optimized for HFO with time-frequency power obtained after spatial filtering optimized for the evoked response.

2.4.6. Decoupling of spontaneous fluctuations in HFO from the evoked response

We were curious whether spinal HFO displayed spontaneous fluctuations in amplitude that were independent from the evoked response, as demonstrated for cortical HFO (Waterstraat et al., 2021). However, unlike the ultra-low noise MEG previously employed to demonstrate such decoupling at the level of cortex, the low signal-to-noise ratio in our recordings prevented reliable estimation of single-trial HFO amplitude. Rather than sorting individual trials into bins with high vs. low HFO power, as in Waterstraat et al. (2021), we therefore randomly resampled from the total number of trials available for each individual and formed sub-averages, which were then sorted according to trial-averaged HFO amplitude. Specifically, in each of 1000 iterations, we randomly drew a subset of 3000 trials for each individual (for the non-invasive recordings; given the lower number of trials, we drew subsets of 1000 trials each in our analysis of invasive recordings). For each subset, we computed power averaged across the time-frequency extent of the cluster previously identified in a group-level, cluster-based permutation test, which compared power in a time-frequency window of interest (200 to 1200 Hz, 8 to 16 ms) to baseline power (200 to 1200 Hz, −100 to −20 ms), across all trials (cluster displayed in Fig. 4, left). For each individual, the two trial subsets with lowest and highest average power were retained. Trials that were common to both subsets were removed from each subset in order to further amplify any difference between subsets. On average, each subset consisted of 2258.8 ± 137.2 trials (mean ± standard deviation; range: 1935 to 2486). For the invasive recordings, 720 trials were available per subset.

We computed single-subject evoked responses for each of these subsets ("low HFO power", "high HFO power"), which were baseline-corrected (−10 to −1 ms) and statistically compared at the group level. A significant difference in HFO power despite no difference in the evoked response would provide evidence of a partial uncoupling of the two signals (Waterstraat et al., 2021). For an optimal signal-to-noise ratio of HFO, and to reduce dimensionality, this analysis was done after projecting data through the DSS filter optimized for HFO (i.e., at the level of the first HFO-DSS component; see Fig. 3A).

To corroborate any lack of a difference in the evoked response, we subjected peak amplitudes, and peak-to-peak amplitudes, to a Bayesian ANOVA. This ANOVA included as one factor the three peaks of the grand-average evoked response (Fig. 1C), or the two inter-peak differences (second minus first peak, and third minus second peak), and as a second factor the two subsets ("low HFO power" vs. "high HFO power"). The resulting 3 × 2 (with peaks as a factor) and 2 × 2 (with inter-peak differences as a factor) Bayesian ANOVAs were computed in JASP (JASP Team, 2019). Single-subject peak latencies for this analysis were identified visually (see also section 2.4.5).

2.4.7. Statistical analysis of EEG data

We used a nonparametric cluster-based permutation test implemented in FieldTrip, which corrects for multiple comparisons across time, frequency, and channels (Maris et al., 2007). Standard FieldTrip settings were used for this test. Adjacent time bins, frequency bins, and channels for which a two-sided, dependent-samples *t*-test provided a *p*-value of < 0.05 were clustered. T-values were summed within each observed cluster to obtain a cluster-level statistic. A distribution under the null hypothesis of no difference (e.g., between baseline and a post-stimulus interval of interest) was obtained by randomly permuting condition labels ("baseline"/"post-stimulus interval") 1000 times, each time computing cluster-level statistics within the observed clusters as described above, and extracting the two clusters with maximum (positive and negative) cluster-level statistics. The cluster-level statistic of each cluster observed in the non-permuted data was then compared to this distribution, and clusters were identified as significant if less than 2.5% of permutations yielded clusters with larger cluster-level statistics. Given our a priori focus on spinal high-frequency signals, we searched for clusters in a time-frequency region of interest between 200 and 1200 Hz, and between 8 and 16 ms after median nerve stimulation. Similarly, cluster-based permutation tests of differences in the evoked response included time points between 8 and 16 ms after median nerve stimulation.

2.5. Data and code availability

Raw EEG data from all healthy individuals, as well as Matlab code, are publicly available on zenodo.org (doi:10.5281/zenodo.6110595).

3. Results

We asked whether high-frequency signals from the human spinal cord, previously detected in invasive, epidural recordings in response to median nerve stimulation (Insola et al., 2008), could also be detected non-invasively via skin electrodes. We also tested whether spinal high-frequency signals carry unique information that is complementary to the spinal evoked response. To this end, separate analyses controlled for phase-locking to stimulation, and tested for a dissociation of high-frequency signals from the evoked response via spatial filtering, and based on their spontaneous dynamics over time.

3.1. Behavior: counting task

In the counting task, healthy volunteers missed, on average, 1.9 ± 1.7 of the 26.8 ± 0.33 omissions present in a block (mean ± SD). There was a significant correlation between true and estimated numbers of omissions in 13 of the 15 healthy volunteers ($p < .01$ after Bonferroni-correction). Similarly, the patient missed, on average 0.4 ± 0.8 of the 18 ± 3.5 omissions present in a block, and we observed a significant correlation between the true and estimated number of omissions in her behavioral data as well ($p < .001$). Reported numbers of omissions thus provided evidence that participants were attending to median nerve stimulation.

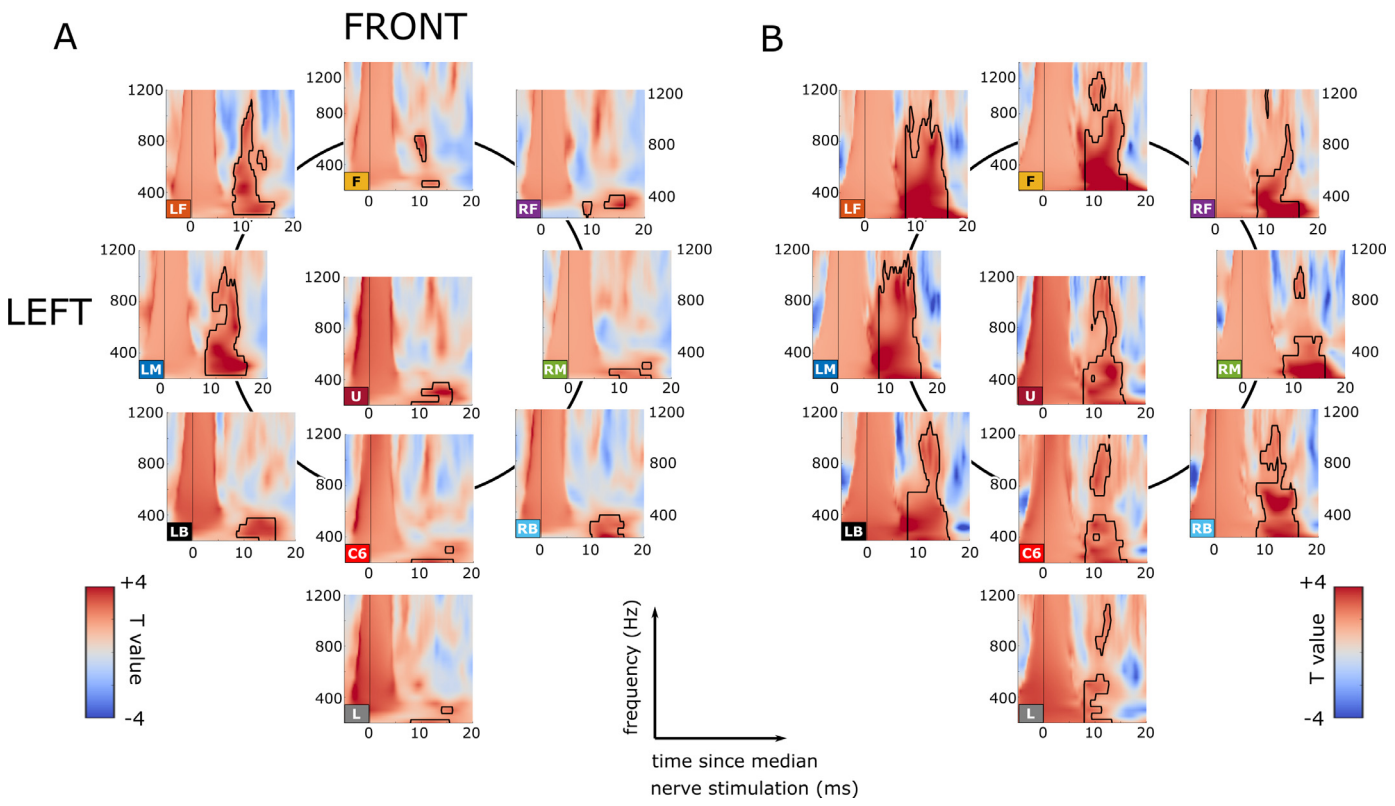

Fig. 2. *Time-frequency representation of the spinal response to electric median nerve stimulation, recorded non-invasively*. ***A***, computed for individual trials, and then averaged across trials. ***B***, computed after averaging across trials (i.e., for the evoked response). Color codes for T values, comparing data to a pre-stimulus baseline (−100 to −20 ms). Insets to individual time-frequency panels (lower left corner) correspond to channel names. The large power increase observed around the time of median nerve stimulation (at time 0, black vertical line) corresponds to the electric stimulation artefact. Black contours indicate the spectral and temporal extent of clusters identified in a cluster-based permutation test (p = .002).

3.2. Grand-average evoked response

Fig. 1C shows the grand-average evoked response to median nerve stimulation across the 15 healthy volunteers. Peak deflections were observed at 9.6, 11.2, and 14 ms (see Restuccia and Mauguière, 1991, for surface recordings of the evoked response using a similar electrode montage). A similar pattern with three peaks at approximately these latencies could be identified in each of the 15 healthy volunteers, confirming that median nerve stimulation was providing effective afferent drive to the spinal cord in each tested individual. Single-subject peak latencies ranged from 8.4 to 10.8 ms for the first peak, from 9.6 to 12.4 ms for the second peak, and from 12.2 to 15.4 ms for the third peak.

3.3. High-frequency signals

Our main interest was in the spectral decomposition of the spinal response to median nerve stimulation. When time- and frequency-resolved power was computed for individual trials, and then averaged across trials, a cluster-based permutation test revealed a significant increase in power above baseline in an *a priori* defined time-frequency window of interest (200 to 1200 Hz, 8 to 16 ms; **Fig. 2A** (T values); black contour: p = .002, cluster-based permutation test; see **Inline Supplementary Results 1** for corresponding time-frequency representations showing percentage change in power). A similar, significant increase above baseline was found when time-frequency power was computed after averaging across individual trials, i.e., in the spectral representation of the evoked response (**Fig. 2B** (T values); black contour: p = .002, cluster-based permutation test).

We next examined whether high-frequency signals in our time-frequency window of interest were purely a spectral representation of the evoked response, or whether they carried information that was partly independent from the evoked response.

3.3.1. Dissociation between high-frequency signals and the evoked response via spatial filters

First, we tested whether a spatial filter that optimized the signal-to-noise ratio of high-frequency signals would result in a submaximal amplitude of the evoked response, compared to a spatial filter that optimized the signal-to-noise ratio of the evoked response, and vice versa. This would rule out the possibility that the observed high-frequency signals are purely a spectral representation of the spinal evoked response. If high-frequency signals were purely a spectral representation of spinal evoked responses, we would expect that their power is maximized when the amplitude of the evoked response is maximized, and vice versa.

To test this, we constructed a spatial filter optimized for signals between 400 and 1200 Hz and between 8 and 16 ms (henceforth labelled "HFO-DSS"). The first HFO-DSS component displayed a significantly higher power-ratio score than would be expected for pure noise, as revealed by a resampling test (**Fig. 3A**; no resampling iteration yielded a stronger power-ratio score, i.e., $p < .001$). The topography of this component showed a lateralization to the left side of the neck, and a bias towards the front of the neck (**Fig. 3A, right**; see **Inline Supplementary Results 2** for a comparison of topographies obtained via a correlation, as in De Cheveigne and Parra, 2014, vs. the inverse of the DSS filter, as described in Haufe et al., 2014).

We then compared high-frequency power after projecting through the HFO-DSS filter (first HFO-DSS component) with high-frequency power after projecting through a DSS filter optimized for the evoked response (see Section 2.4.5; henceforth labelled "ERP-DSS"). Our goal was to examine whether a spatial filter that maximized the signal-to-

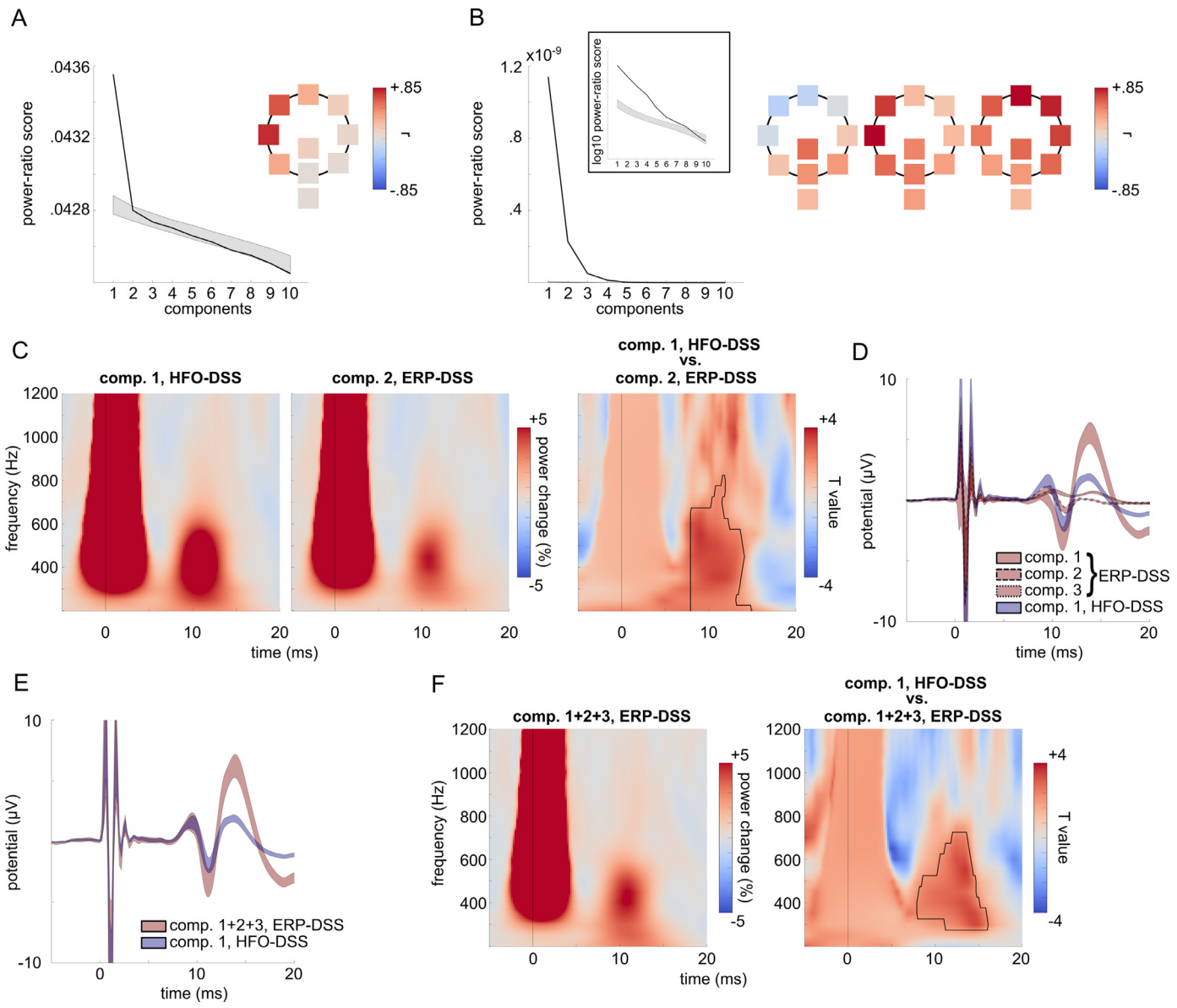

Fig. 3. *Dissociation of high-frequency signals and the evoked response via spatial filtering.* ***A***, power-ratio score for each of the ten components of a DSS filter optimized for high-frequency power between 400 and 1200 Hz and 8 to 16 ms (HFO-DSS). The gray shading represents 95% confidence intervals of power-ratio scores obtained in a resampling test. The topography of the first DSS component is displayed on the right (same schematic outline as in Fig. 1C). Color represents correlation coefficients of the first DSS component with unfiltered data at each of the ten channels. ***B***, same as *A*, but for a DSS filter optimized for the evoked response (ERP-DSS). The inset shows power-ratio scores after log-transformation, so that "true" power-ratio scores can be visually compared to the distribution under the null hypothesis of a resampling test (gray shading). Topographies of the first three ERP-DSS components are displayed on the right. ***C***, time- and frequency-resolved changes in power, relative to a pre-stimulus baseline (−100 to −20 ms) for the first HFO-DSS component (left), and for the second ERP-DSS component (right; i.e., the ERP-DSS component with the highest power between 200 and 1200 Hz, and 8 to 16 ms). The right panel shows T values comparing the two components. The black contour represents the spectral and temporal extent of a cluster identified in a cluster-based permutation test ($p = 0.002$). ***D***, Grand-average evoked responses (± standard error of the mean) of the first three ERP-DSS components, and the first HFO-DSS component. ***E***, Grand-average evoked responses (± standard error of the mean) of the sum of the first three ERP-DSS components, and of the first HFO-DSS component. ***F***, time- and frequency-resolved changes in power, relative to a pre-stimulus baseline (−100 to −20 ms) for the sum of the first three ERP-DSS components (left). The right panel shows T values comparing time- and frequency-resolved power between the first HFO-DSS component (left in *C*) and the sum of the first three ERP-DSS components. The black contour represents the spectral and temporal extent of a cluster identified in a cluster-based permutation test ($p = .008$).

noise ratio of the evoked response (ERP-DSS) would be suboptimal for detecting HFO, and vice versa. This would provide evidence that the amplitudes of the two signals are dissociable.

ERP-DSS yielded eight components whose power-ratio scores were significantly higher than would be expected for pure noise (Fig. 3**B**). Of these eight components, the second displayed the highest power in our time-frequency window of interest. Still, we found that high-frequency power of this second component was significantly lower than high-frequency power obtained after projecting through the HFO-DSS filter (first HFO-DSS component; Fig. 3**C**; $p = .002$; cluster-based permutation test).

A cluster-based permutation test also revealed significant differences between evoked responses obtained after projecting through the two filters. Specifically, the third peak of the evoked response was higher in amplitude for the first ERP-DSS component, compared to the first HFO-DSS component ($p = .002$). The first peak of the evoked response, on the

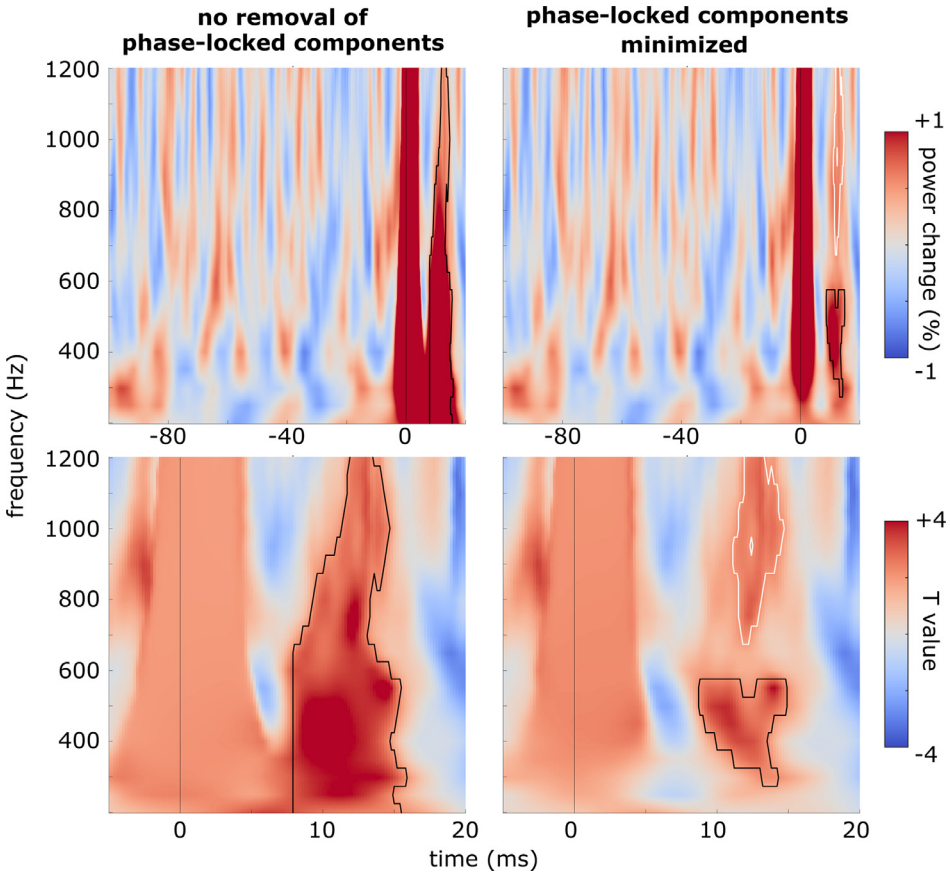

Fig. 4. *Phase-locking of high-frequency signals*. The left column shows time- and frequency-resolved power changes from baseline (top) and T values against baseline (bottom) of the first HFO-DSS component without subtraction of phase-locked responses. The right column shows the same, but after mean Fourier spectra across trials were subtracted from single-trial Fourier spectra before computing power, thus minimizing phase-locked responses. The top row shows power change across an extended time interval to allow inspection of the time window chosen as a baseline (−100 to −20 ms). Black and white contours show the spectral and temporal extent of clusters identified in a cluster-based permutation test (p = .002 (left column), p = .014 (right column, black), and p = .022 (right column, white)). The top left panel shows the same data as Fig. 3C, left, however, with a different color scale that facilitates visual comparison with the top right panel (in addition to the abovementioned extended time axis).

other hand, was *lower* in amplitude for the first ERP-DSS component, compared to the first HFO-DSS component (**Fig. 3D**; p = .002). A likely reason for this is that the ERP-DSS filter represented the evoked response by eight different components (Fig. 3B). We therefore examined whether summing several ERP-DSS components would yield amplitudes of each of the three peaks of the evoked response that are at least as large as the evoked response obtained from the first HFO-DSS component. If the observed high-frequency signals were purely a spectral representation of the evoked response, then comparable or even higher amplitudes of the evoked response due to summing of ERP-DSS components should result in comparable or even larger high-frequency power than observed for the first HFO-DSS component. If, on the other hand, the first HFO-DSS component still displayed a larger increase in high-frequency power than this sum of ERP-DSS components, then this increase could not be explained purely as a spectral representation of the evoked response. This would reveal the presence of a high-frequency signal whose power is dissociable from the amplitude of the evoked response.

Summing the first three ERP-DSS components was sufficient to abolish the significant decrease in the amplitude of the first peak of the evoked response when compared to the first HFO-DSS component (**Fig. 3E**; p > .1 for any decrease in amplitude; p = .002 for an increase in amplitude around the time of the third peak; cluster-based permutation test). Instead, when comparing amplitudes of the first and second peak at subject-specific peak latencies between the first HFO-DSS component and the sum of the first three ERP-DSS components, we found that the latter yielded significantly higher peak amplitudes ($t(14) = 2.6$, p = .04, for the first peak, and $t(14) = 6.6$, p < .001, for the second peak; Bonferroni-corrected (2 tests); see **Inline Supplementary Results 3** for single-subject evoked responses, together with visually identified peak latencies). Summing the first three ERP-DSS components thus yielded an evoked response whose three peaks had larger amplitudes than observed for the first HFO-DSS component.

Importantly, however, the significant increase in high-frequency power for the first HFO-DSS component, compared to the ERP-DSS components, persisted even after summing the first three ERP-DSS components (**Fig. 3F**; p = .008), i.e., despite the significantly lower amplitudes of the evoked response observed for the first HFO-DSS component.

3.3.2. *Phase-locking of high-frequency signals*

Second, we examined to what extent this increase in high-frequency power was phase-locked to median nerve stimulation. To this end, we subtracted, for each individual, the mean across complex-valued Fourier spectra across trials from single-trial complex-valued Fourier spectra before computing power, and then averaged power across trials. Taking advantage of the increase in signal-to-noise ratio by spatial filtering, this was done for the first HFO-DSS component. While subtraction of phase-locked components substantially decreased high-frequency power (**Fig. 4**, left vs. right), a significant increase in power above baseline persisted even after subtraction of phase-locked responses (black and white contours in Fig. 4, right; black contour: p = .014; white contour: p = .022; cluster-based permutation test).

3.3.3. *Decoupling of spontaneous fluctuations in HFO from the evoked response*

Third, we tested whether high-frequency power displayed spontaneous fluctuations in the absence of any concurrent, systematic change in the amplitude of the evoked response. To this end, we identified subsets of trials which differed significantly in high-frequency power (p = .002; cluster-based permutation test between 200 and 1200 Hz, and 8 to 16 ms; **Fig. 5A**; for an optimal signal-to-noise ratio of HFO, and to reduce dimensionality, we focused on the first HFO-DSS component, see Fig. 3A). Importantly, despite this significant difference in high-frequency power, the same trial subsets did not differ significantly in their evoked responses (no clusters identified in a cluster-based per-

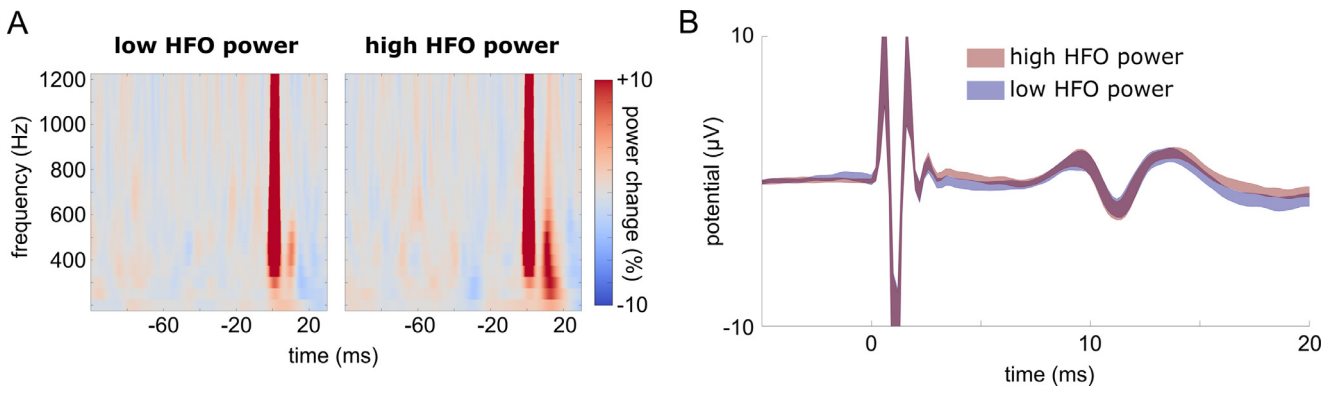

Fig. 5. *Decoupling of spontaneous fluctuations in high-frequency power from the evoked response.* ***A***, change in power from baseline for two trial subsets chosen to minimize (left) and maximize (right) power between 200 and 1200 Hz, and 8 to 16 ms. ***B***, grand-average evoked response (± standard error of the mean) for the two trial subsets shown in *A*.

mutation test, 8 to 16 ms; Fig. 5**B**). A Bayesian ANOVA provided evidence that there was indeed no difference in the evoked response when HFO power was high vs. low for any of the three peaks (subject-specific peak latencies, see Inline Supplementary Results 3; BF_{excl} = 5.8 for the factor "trial subset", and BF_{excl} = 8 for the interaction between "trial subset" and "peak") or any of the two inter-peak differences (i.e., between peak 1 and 2, and between peak 2 and 3; BF_{excl} = 4.4 for the factor "trial subset", and BF_{excl} = 3,4 for the interaction between "trial subset" and "inter-peak difference"). We confirmed these results in a separate analysis which controlled for differences in baseline power between trial subsets (see **Inline Supplementary Results 4**).

3.3.4. High-frequency signals in epidural recordings

This increase in power between 200 and 1200 Hz, and between 8 to 16 ms, observed in non-invasive cervical recordings overlapped in frequency and latency with a signal observed in epidural recordings from the cervical spinal cord in a patient with neuropathic pain (Fig. 6). Here, we also observed a significant increase in power above baseline in our time-frequency window of interest between 200 and 1200 Hz, and between 8 and 16 ms (black contours in Fig. 6A: p = .016, and p = .02, cluster-based permutation test). Similar to the non-invasive recordings, this high-frequency signal fluctuated in amplitude at least partly independently from the evoked response. Specifically, despite a significant difference in high-frequency power between randomly defined trial subsets (p = .002, cluster-based permutation test; Fig. 6**B**), we found no significant difference in the evoked response between these two subsets (no clusters identified in a cluster-based permutation test; Fig. 6**C**). A Bayesian independent-samples T test comparing peak amplitudes of the evoked response provided evidence that the evoked response did, indeed, not differ when high-frequency power was high vs. low (BF = 14.7).

3.3.5. Single-subject high-frequency signals in non-invasive recordings

Finally, we examined single-subject time-frequency representations for inter-individual consistency of a short-latency, high-frequency (~200–1200 Hz, 8–16 ms) signal. An increase in power was observed in the majority of healthy volunteers (Fig. 7).

4. Discussion

We report three findings. First, non-invasive recordings of electrophysiological signals via skin electrodes placed around the neck reveal high-frequency signals between 200 and 1200 Hz, and between 8 and 16 ms after median nerve stimulation. Second, while the spectro-temporal representation of the evoked response, too, shows an increase in power in this time-frequency window, we demonstrate that high-frequency signals can be dissociated from the evoked response. Specifically, we show that spatial filters optimized for the evoked response cannot fully capture the observed high-frequency signal, i.e., significantly less than a spatial filter optimized for these high-frequency signals. We also demonstrate uncoupling of spontaneous fluctuations in the amplitude of high-frequency signals from the evoked response. In addition, an increase in high-frequency power following median nerve stimulation persists after minimizing phase-locked responses. Third, the observed high-frequency signal overlaps in latency and, partly, in frequency range with a signal recorded epidurally in response to median nerve stimulation. We discuss possible generators underlying these short-latency HFO, their potential to provide complementary information to the evoked response, including a possible window onto pathophysiology, benefits of non-invasive recordings in this regard, and limitations of our study, together with potential future directions.

Since their description in scalp recordings (Cracco and Cracco, 1976; Eisen et al., 1984; Yamada et al., 1988; Emori et al., 1991), it has been shown that HFO (~600 Hz), elicited by electric median nerve stimulation, are at least partly independent from the concurrent evoked response. Compared to the N20, HFO show different dynamics when comparing sleep and wakefulness (Hashimoto et al., 1996), when opening the eyes (Gobbelé et al., 2000; but see Restuccia et al., 2004), during hyperventilation (Mochizuki et al., 2003), as a function of stimulation rate (Klostermann et al., 1999b), tactile interference stimulation (Hashimoto et al., 1999), and movement (Klostermann et al., 2001a). HFO thus carry information that is complementary to evoked responses. The N20 is considered a population measure of (excitatory) post-synaptic potentials (Wikström et al., 1996), in line with the idea that signals < ~100 Hz reflect mass synaptic input (Logothetis, 2003). HFO, on the other hand, have been associated with neuronal spiking. Baker et al. (2003) have shown that single-unit bursts and individual spikes in S1 of macaque monkeys are phase-locked to ~600 Hz signals recorded epidurally in response to median nerve stimulation. Such phase-locking was confirmed by Telenczuk et al. (2011), who additionally observed a correlation between trial-to-trial variability in single-cell spiking in S1 on the one hand, and trial-to-trial variability in epidurally recorded HFO on the other. Together, these findings suggest that HFO represent a population measure related to neuronal spiking. Some authors have therefore labelled HFO as "spike-like" (Gobbelé et al., 1999; Klostermann et al., 2001a, 2001b; Fedele et al., 2015).

The possibility to obtain information about neuronal spiking in the human nervous system via population signals has inspired research into HFO also at subcortical sites. Invasive recordings from (sub)thalamus via deep brain stimulation (DBS) electrodes (Klostermann et al., 1999a; Insola et al., 2015), and from brainstem via DBS electrodes (Insola et al., 2014), epidural electrodes (Insola et al., 2010), or nasopharyngeal electrodes (Restuccia et al., 2004), have revealed HFO in response to median nerve stimulation also at these subcortical sites. Similar to scalp record-

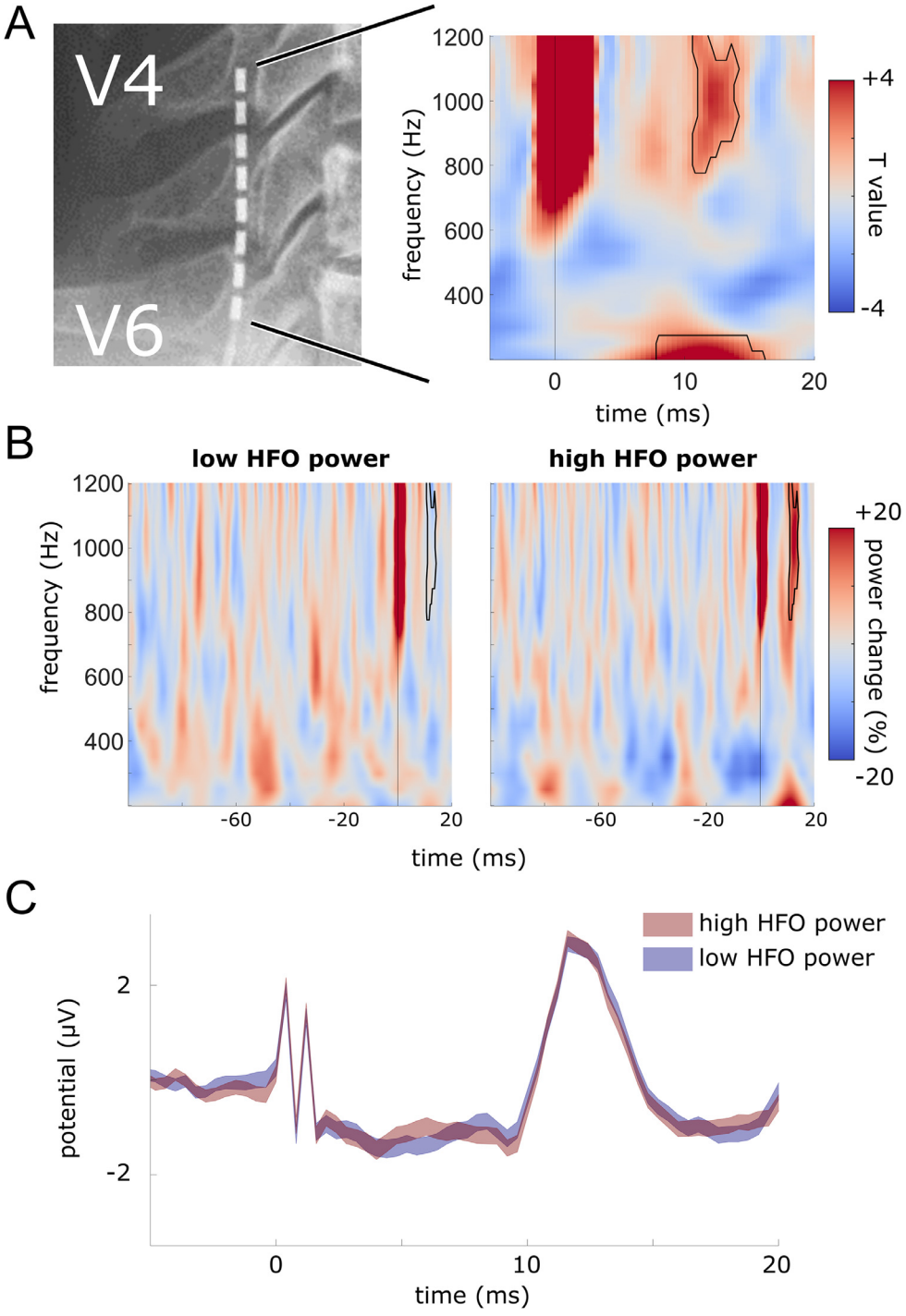

Fig. 6. *Epidural electrode location, and time-frequency representation of the spinal response to electric median nerve stimulation, recorded invasively*. ***A***, *left*, X-ray of electrode placement. V4 and V6, spinous processes of vertebrae 4 and 6. *Right*, T values comparing time- and frequency-resolved power to a pre-stimulus baseline (−100 to −20 ms). The large power increase observed around the time of median nerve stimulation (at time 0, black vertical line) corresponds to the electric stimulation artefact. Black contours indicate the spectral and temporal extent of clusters identified in a cluster-based permutation test (p = .016 and p = .02). ***B***, change in power from baseline for two trial subsets chosen to minimize (left) and maximize (right) power between 200 and 1200 Hz, and 8 to 16 ms. The black contour corresponds to the cluster identified in panel *A*, right. ***C***, evoked response (± standard error of the mean, across trials) for the two trial subsets shown in *B*.

ings of longer-latency HFO, these invasive recordings have also confirmed a partial independence between HFO and the evoked response (Klostermann et al., 1999a; Restuccia et al., 2004).

With the exception of nasopharyngeal recordings, these invasive recordings are confined to a context of pathology, medication, and surgery, and often to relatively small cohorts. This may limit the generalizability of findings from invasive recordings. HFO are abnormal in several clinical disorders, including disorders treated via DBS. For example, HFO at the scalp are enlarged in patients with Parkinson's Disease (Mochizuki et al., 1999; Inoue et al., 2001), and diminished in patients with cervical dystonia (Inoue et al., 2004). It is therefore possible that invasive recordings of subcortical HFO in these disorders, and possibly others, do not reflect the normal physiology of these signals in the healthy nervous system.

A restriction to invasive recordings has also been a likely reason for the low number of studies into HFO at the earliest possible stage of somatosensory processing in the human central nervous system, i.e., in the spinal cord. Based on recordings from epidural electrodes implanted alongside the cervical spinal cord for pain relief, Insola et al. (2008) reported high-frequency signals in response to median nerve stimulation. The latency of these signals, starting at 9.8 ms, and the close proximity of the electrode to the spinal cord, pointed to spinal generators for these signals. Specifically, two different high-frequency signals were identified: A lower-frequency signal, with a mean frequency of ~500 Hz,

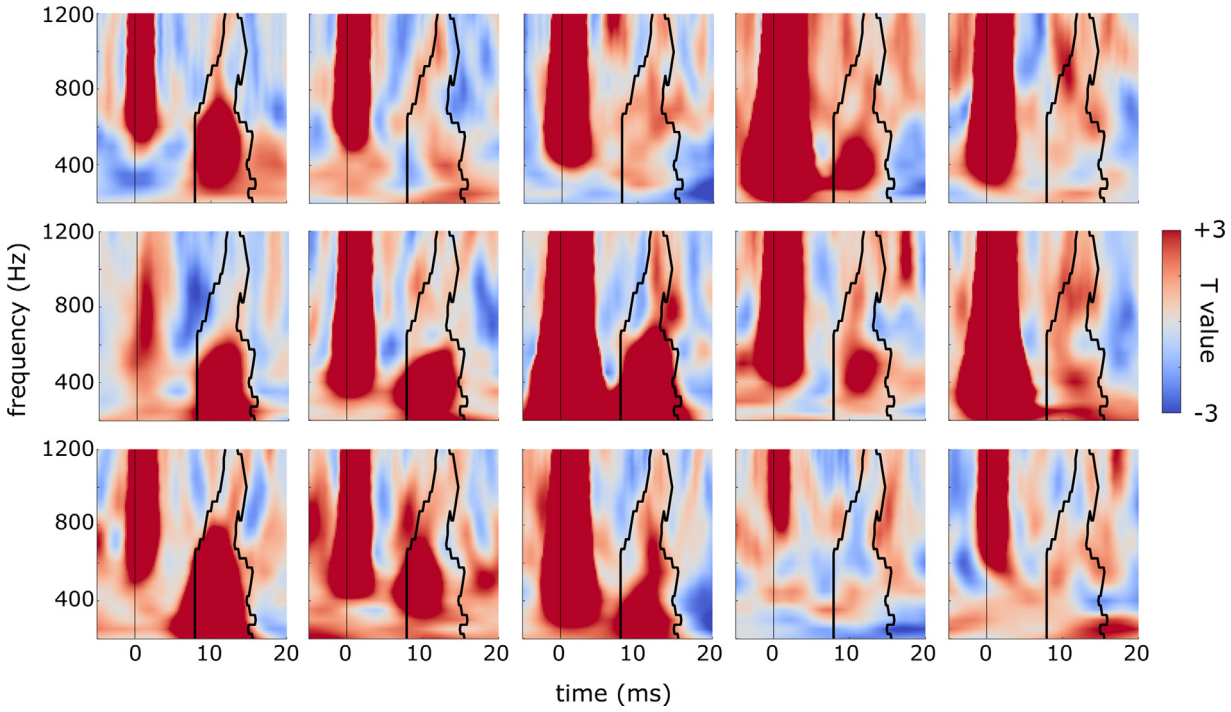

Fig. 7. *Single-subject spectral power in response to median nerve stimulation, recorded non-invasively*. Each panel corresponds to data from one healthy volunteer (first HFO-DSS component). Color codes for T values comparing power to a pre-stimulus baseline, within subjects. The black contour indicates the spectral and temporal extent of the cluster identified in a cluster-based permutation test at the group level (i.e., identical to Fig. 4, bottom-left panel).

which was not attenuated during movement of the ipsilateral wrist; and a higher-frequency signal, with a mean frequency of ~1200 Hz, which did show this attenuation, as did the evoked response. Based on the assumption that gating through movement acts on post-synaptic potentials (but see Seki et al., 2003), Insola et al. (2008) argued that the higher-frequency signal around 1200 Hz represents a post-synaptic signal from the spinal dorsal horn.

Here, we replicate a similar, higher-frequency (~1000 Hz) power increase in response to median nerve stimulation in epidural recordings from the cervical spinal cord. Importantly, we also show that HFO can be recorded non-invasively, via skin electrodes placed around the neck, and at latencies that are similar to those reported by Insola et al. (2008). Our study thus demonstrates the feasibility of recording HFO at very short latencies non-invasively in humans, circumventing potential confounds that arise in a context of pathology, medication, and surgery. Given that the maximum cut-off frequency of the anti-aliasing low-pass filter of our equipment was 1000 Hz, we were reluctant to examine signals > 1200 Hz, limiting comparison of results with Insola et al. (2008).

Previous research has distinguished HFO at ~500–600 Hz from HFO at ~1000 Hz for supra-spinal regions. The former are sometimes called σ-bursts (Curio, 2000), and the latter κ-bursts (Fedele et al., 2015). Signals in the frequency range of κ-bursts have been reported in thalamus (Hanajima et al., 2004, 2006), as well as in low-noise, non-invasive scalp recordings (Fedele et al., 2015). Together with Insola et al. (2008), our study demonstrates that signals in the range of σ- and κ-bursts can also be recorded at latencies indicative of spinal processing. Curio has argued that signals at 12–14 ms after median nerve stimulation may originate from cuneothalamic relay neurons, i.e.,. from the lower brainstem. Time-frequency analysis entails some degree of uncertainty about signal latencies. However, given that local, epidural recordings from the dorsal cervical spinal cord reveal short-latency HFO, both in our study, as well as in Insola et al. (2008), we conclude, like Insola et al. (2008), that these short-latency signals originate in the spinal cord.

Why have previous studies into HFO that included cervical skin electrodes not detected the signals reported here? Coppola et al. (2005), for example, reported peak latencies of HFO ~16–17 ms, even though their study included a cervical electrode. Apart from their focus on a relatively low frequency range (450–750 Hz) and on phase-locked signals, they only included one cervical electrode (on the fifth cervical spinous process). In this regard, it may be critical to include electrodes on the lateral portion of the neck, given that LM and LF showed the largest signal in our study (Fig. 2). Whether this reflects a true lateralization relative to the side of stimulation remains to be tested. If so, non-invasive recordings may reveal additional, important information about laterality of spinal processing.

Non-invasive recordings of HFO from the spinal cord provide a novel window onto physiological and pathophysiological mechanisms of somatosensory pre-processing in the spinal cord. It is unclear how spinal HFO relate to natural somatosensory input, such as touch, or to proprioceptive or nociceptive input. Spinal gating has been long associated with pain control (Melzack and Wall, 1965; Guo and Hu, 2014), and, more recently, freezing of gait in Parkinson's disease (Lira et al., 2020). Non-invasive neck recordings may help elucidate the role of HFO in these processes. Furthermore, previous studies using functional imaging of the cervical spinal cord have demonstrated an involvement of the human spinal cord in placebo and nocebo effects, i.e., effects of prior belief/expectation, as well as attention effects on nociceptive pain (Eippert et al., 2009; Sprenger et al., 2012; Geuter and Büchel, 2013). Functional imaging lacks the temporal resolution to clarify whether this spinal involvement in expectation and attention relates to feedforward, or feedback processes. Non-invasive recordings of spinal HFO may help clarify this issue, given their high temporal resolution.

One limitation of our study is the relatively low cut-off frequency of the anti-aliasing low-pass filter of our equipment, which we had set to the maximum possible cut-off frequency (1000 Hz). This cut-off frequency prevented us from investigating signals >1200 Hz, unlike Insola et al. (2008), and may have caused us to underestimate spectral power between 1000 and 1200 Hz. Amplifiers with a higher cut-off frequency are commercially available, and may reveal the full spectral extent of HFO in non-invasive neck recordings.

Furthermore, while our study shows the feasibility of recording high-frequency signals using standard, commercially available EEG equipment, this equipment is likely not optimal for detecting signals in the range of several hundred Hz, whose signal-to-noise ratio is typically strongly influenced by thermal and electronic noise determined by the experimental equipment (Scheer et al., 2006). Such noise plays little or no role when analysing neural signals at lower frequencies (e.g., below 100 Hz). However, due to the 1/f spectral pattern of neurophysiological data, high-frequency signals in the range of several hundred Hz can fall below such equipment noise. Research into cortical high-frequency signals has demonstrated benefits of using low-noise EEG equipment (Waterstraat et al., 2012, 2015; Fedele et al., 2015). Recordings of spinal high-frequency signals, too, would likely profit from such low-noise equipment.

A second potential limitation is that our approach to minimize phase-locked responses relies on estimation of phase, which, in turn, is vulnerable to low power (Van Diepen and Mazaheri, 2018). Given that the observed HFO signals in our study were low in amplitude, estimation of phase, and therefore removal of phase-locked responses, may not have been complete. In addition, a finite sampling frequency imposes limitations on how consistently even highly phase-locked signals are recorded across repetitions. Indeed, "removal" of phase-locked components in our study did not fully abolish the stimulation artefact (Fig. 4), i.e., a signal that is highly phase-locked.

However, our conclusion that the observed HFO signals are at least partly dissociable from the evoked response, does not rest exclusively on their incomplete phase-locking. In addition, we show that the observed high-frequency signals are dissociable from the evoked response via spatial filtering, and in their spontaneous dynamics over time. Our comparison of high-frequency power, and evoked response amplitude, between HFO-DSS and ERP-DSS filters provides no evidence of a spatial dissociation of the two signals. However, this comparison did show that a spatial filter optimized for the evoked response cannot fully capture the observed high-frequency signals, ruling out the possibility that high-frequency signals are purely a spectral representation of the evoked response. A higher density of electrodes placed around the neck may further help in constructing signal-specific spatial filters in the future. In addition, future studies may address the functional significance of the spontaneous fluctuations in high-frequency power observed in our study, which were at least partly independent of the evoked response.

In summary, we provide first evidence that high-frequency signals can be recorded non-invasively, via surface electrodes around the neck, at latencies that are indicative of a spinal source. Importantly, the non-invasive nature of our recording protocol allows for testing HFO in healthy individuals, circumventing limitations of previous, invasive studies to contexts of pathology, medication, and surgery. We further show a dissociation between HFO and the evoked response. Our recording protocol thus provides a novel window onto the physiology, and pathophysiology, of the human spinal cord.

Funding

M.-P. Stenner was supported by a VolkswagenStiftung Freigeist Fellowship, project-ID 92977, and received funding from a Deutsche Forschungsgemeinschaft Sonderforschungsbereich, SFB-1436, TPC03, project-ID 425899996.

Data and code availability

Raw EEG data from all healthy individuals, as well as Matlab code, are publicly available on zenodo.org (doi:10.5281/zenodo.6110595).

Declaration of Competing Interest

The authors declare no competing financial interests.

Credit authorship contribution statement

Bankim Subhash Chander: Formal analysis, Investigation, Data curation, Writing – original draft, Visualization. **Matthias Deliano:** Conceptualization, Resources, Validation, Investigation, Writing – review & editing. **Elena Azañón:** Validation, Writing – review & editing. **Lars Büntjen:** Validation, Resources, Writing – review & editing. **Max-Philipp Stenner:** Conceptualization, Validation, Software, Formal analysis, Visualization, Supervision, Funding acquisition, Writing – original draft, Resources, Project administration.

Acknowledgements

We thank all participants for their time and effort, and two anonymous reviewers for their valuable comments and suggestions.

Supplementary materials

Supplementary material associated with this article can be found, in the online version, at doi:10.1016/j.neuroimage.2022.119050.

References

Arnal, L.H., Giraud, A.L., 2012. Cortical oscillations and sensory predictions. Trends Cogn. Sci. 16, 390–398. Available at http://www.ncbi.nlm.nih.gov/pubmed/22682813. [Accessed November 8, 2013].

Baker, S.N., Curio, G., Lemon, R.N., 2003. EEG oscillations at 600Hz are macroscopic markers for cortical spike bursts. J. Physiol. 550, 529–534.

Bauer, M., Kluge, C., Bach, D., Bradbury, D., Heinze, H.J., Dolan, R.J., Driver, J., 2012. Cholinergic enhancement of visual attention and neural oscillations in the human brain. Curr. Biol. 22, 397–402. CBAvailable at http://www.pubmedcentral.nih.gov/articlerender.fcgi?artid=3314945&tool=pmcentrez&rendertype=abstract. [Accessed July 17, 2012].

Buzsáki, G., Andreas, D., Draguhn, A., 2004. Neuronal oscillations in cortical networks. Science 304, 1926. (80-)Available at http://www.ncbi.nlm.nih.gov/pubmed/15218136.

Coppola, G., Vandenheede, M., Di Clemente, L., Ambrosini, A., Fumal, A., De Pasqua, V., Schoenen, J., 2005. Somatosensory evoked high-frequency oscillations reflecting thalamo-cortical activity are decreased in migraine patients between attacks. Brain 128, 98–103.

Cracco, R.Q., Cracco, J.B., 1976. Somatosensory evoked potential in man: far field potentials. Electroencephalogr. Clin. Neurophysiol. 41, 460–466.

Curio, G., 2000. Linking 600-Hz "spikelike" EEG/MEG wavelets ("sigma-Bursts") to cellular substrates. J. Clin. Neurophysiol. 17, 1–20 Available at: papers://2e0d27ab-c3fe-4d7f-898d-5ff9ff75f50b/Paper/p2.

Curio, G., Mackert, B.M., Burghoff, M., Koetitz, R., Abraham-Fuchs, K., Härer, W., 1994. Localization of evoked neuromagnetic 600 Hz activity in the cerebral somatosensory system. Electroencephalogr. Clin. Neurophysiol. 91, 483–487.

Curio, G., Mackert, B.M., Burghoff, M., Neumann, J., Nolte, G., Scherg, M., Marx, P., 1997. Somatotopic source arrangement of 600 Hz oscillatory magnetic fields at the human primary somatosensory hand cortex. Neurosci. Lett. 234, 131–134.

De Cheveigne, A., Parra, L.C., 2014. Joint decorrelation, a versatile tool for multichannel data analysis. Neuroimage 98, 487–505. doi:10.1016/j.neuroimage.2014.05.068, Available at:.

Eippert, F., Finsterbusch, J., Bingel, U., Büchel, C., 2009. Direct evidence for spinal cord involvement in placebo analgesia. Science 326, 404.

Eisen, A., Roberts, K., Low, M., Hoirch, M., Lawrence, P., 1984. Questions regarding the sequential neural generator theory of the somatosensory evoked potential raised by digital filtering. Electroencephalogr. Clin. Neurophysiol. 59, 388–395.

Emori, T., Yamada, T., Seki, Y., Yasuhara, A., Ando, K., Honda, Y., Leis, A.A., Vachatimanont, P., 1991. Recovery functions of fast frequency potentials in the initial negative wave of median SEP. Electroencephalogr. Clin. Neurophysiol. 78, 116–123.

Fedele, T., Scheer, H.J., Burghoff, M., Curio, G., Körber, R., 2015. Ultra-low-noise EEG/MEG systems enable bimodal non-invasive detection of spike-like human somatosensory evoked responses at 1 kHz. Physiol. Meas. 36, 357–368. doi:10.1088/0967-3334/36/2/357, Available at.

Geuter, S., Büchel, C., 2013. Facilitation of pain in the human spinal cord by nocebo treatment. J. Neurosci. 33, 13784–13790. Available at http://www.ncbi.nlm.nih.gov/pubmed/23966699.

Gobbelé, R., Buchner, H., Scherg, M., Curio, G., 1999. Stability of high-frequency (600 Hz) components in human somatosensory evoked potentials under variation of stimulus rate-evidence for a thalamic origin. Clin. Neurophysiol. 110, 1659–1663.

Gobbelé, R., Waberski, T.D., Kuelkens, S., Sturm, W., Curio, G., Buchner, H., 2000. Thalamic and cortical high-frequency (600 Hz) somatosensory-evoked potential (SEP) components are modulated by slight arousal changes in awake subjects. Exp. Brain Res. 133, 506–513.

Guo, D., Hu, J., 2014. Spinal presynaptic inhibition in pain control. Neuroscience 283, 95–106.

Hanajima, R., Chen, R., Ashby, P., Lozano, A.M., Hutchison, W.D., Davis, K.D., Dostrovsky, J.O., 2004. Very fast oscillations evoked by median nerve stimulation in the human thalamus and subthalamic nucleus. J. Neurophysiol. 92, 3171–3182.

Hanajima, R., Dostrovsky, J.O., Lozano, A.M., Chen, R., 2006. Dissociation of thalamic high frequency oscillations and slow component of sensory evoked potentials following damage to ascending pathways. Clin. Neurophysiol. 117, 906–911.

Hashimoto, I., Kimura, T., Fukushima, T., Iguchi, Y., Saito, Y., Terasaki, O., Sakuma, K., 1999. Reciprocal modulation of somatosensory evoked N20m primary response and high-frequency oscillations by interference stimulation. Clin. Neurophysiol. 110, 1445–1451.

Hashimoto, I., Mashiko, T., Imada, T., 1996. Somatic evoked high-frequency magnetic oscillations reflect activity of inhibitory interneurons in the human somatosensory cortex. Electroencephalogr. Clin. Neurophysiol. 100, 189–203 Evoked Potentials.

Haufe, S., Meinecke, F., Görgen, K., Dähne, S., Haynes, J.D., Blankertz, B., Bießmann, F., 2014. On the interpretation of weight vectors of linear models in multivariate neuroimaging. Neuroimage 87, 96–110. doi:10.1016/j.neuroimage.2013.10.067, Available at.

Herreras, O., 2016. Local field potentials: myths and misunderstandings. Front. Neural Circuits 10, 1–16.

Inoue, K., Hashimoto, I., Nakamura, S., 2001. High-frequency oscillations in human posterior tibial somatosensory evoked potentials are enhanced in patients with Parkinson's disease and multiple system atrophy. Neurosci. Lett. 297, 89–92.

Inoue, K., Hashimoto, I., Shirai, T., Kawakami, H., Miyachi, T., Mimori, Y., Matsumoto, M., 2004. Disinhibition of the somatosensory cortex in cervical dystonia - Decreased amplitudes of high-frequency oscillations. Clin. Neurophysiol. 115, 1624–1630.

Insola, A., Padua, L., Mazzone, P., Scarnati, E., Valeriani, M., 2014. Low and high-frequency somatosensory evoked potentials recorded from the human pedunculopontine nucleus. Clin. Neurophysiol. 125, 1859–1869. doi:10.1016/j.clinph.2013.12.112, Available at.

Insola, A., Padua, L., Mazzone, P., Valeriani, M., 2008. Unmasking of presynaptic and postsynaptic high-frequency oscillations in epidural cervical somatosensory evoked potentials during voluntary movement. Clin. Neurophysiol. 119, 237–245.

Insola, A., Padua, L., Mazzone, P., Valeriani, M., 2010. Effect of movement on SEPs generated by dorsal column nuclei. Clin. Neurophysiol. 121, 921–929. doi:10.1016/j.clinph.2010.01.006, Available at.

Insola, A., Padua, L., Mazzone, P., Valeriani, M., 2015. Low- and high-frequency subcortical SEP amplitude reduction during pure passive movement. Clin. Neurophysiol. 126, 2366–2375. doi:10.1016/j.clinph.2015.03.021, Available at.

Klostermann, F., Funk, T., Vesper, J., Curio, G., 1999a. Spatiotemporal characteristics of human intrathalamic high-frequency (>400Hz) SEP components. Neuroreport 10, 3627–3631.

Klostermann, F., Gobbele, R., Buchner, H., Siedenberg, R., Curio, G., 2001a. Differential gating of slow postsynaptic and high-frequency spike-like components in human somatosensory evoked potentials under isometric motor interference. Brain Res. 922, 95–103.

Klostermann, F., Nolte, G., Curio, G., 1999b. Multiple generators of 600Hz wavelets in human SEP unmasked by varying stimulus rates. Neuroreport 10, 1625–1629.

Klostermann, F., Nolte, G., Curio, G., 2001b. Independent short-term variability of spike–like (600 Hz) postsynaptic (N20) cerebral ESP components. Neuroreport 12, 349–352.

Lira, J.L.O., Ugrinowitsch, C., Coelho, D.B., Teixeira, L.A., de Lima-Pardini, A.C., Magalhães, F.H., Barbosa, E.R., Horak, F.B., Silva-Batista, C., 2020. Loss of presynaptic inhibition for step initiation in parkinsonian individuals with freezing of gait. J. Physiol. 8, 1611–1624.

Logothetis, N.K., 2003. The underpinnings of the BOLD functional magnetic resonance imaging signal. J. Neurosci. Off. J. Soc. Neurosci. 23, 3963–3971. Available at http://www.ncbi.nlm.nih.gov/pubmed/12764080.

Maris, E., Schoffelen, J.M., Fries, P., 2007. Nonparametric statistical testing of coherence differences. J. Neurosci. Methods 163, 161–175. Available at http://www.ncbi.nlm.nih.gov/pubmed/17395267. [Accessed September 17, 2013].

Melzack, R., Wall, P., 1965. Pain mechanism: a new theory. Science 150, 971–979 (80-).

Mochizuki, H., Machii, K., Terao, Y., Furubayashi, T., Hanajima, R., Enomoto, H., Uesugi, H., Shiio, Y., Kamakura, K., Kanazawa, I., Ugawa, Y., 2003. Recovery function of and effects of hyperventilation on somatosensory evoked high-frequency oscillation in Parkinson's disease and myoclonus epilepsy. Neurosci. Res. 46, 485–492.

Mochizuki, H., Ugawa, Y., Machii, K., Terao, Y., Hanajima, R., Furubayashi, T., Uesugi, H., Kanazawa, I., 1999. Somatosensory evoked high-frequency oscillation in Parkinson's disease and myoclonus epilepsy. Clin. Neurophysiol. 110, 185–191.

Moreland, K., 2009. Diverging color maps for scientific visualization. In: Advances in Visual Computing. ISVC 2009. Lecture Notes in Computer Science, Berlin, Heidelberg, pp. 92–103 Available at.

Oostenveld, R., Fries, P., Maris, E., Schoffelen, J..M., 2011. FieldTrip: open source software for advanced analysis of MEG, EEG, and invasive electrophysiological data. Comput. Intell. Neurosci. 2011, 156869. Available at http://www.pubmedcentral.nih.gov/articlerender.fcgi?artid=3021840&tool=pmcentrez&rendertype=abstract. [Accessed July 13, 2012].

Ozaki, I., Hashimoto, I., 2011. Exploring the physiology and function of high-frequency oscillations (HFOs) from the somatosensory cortex. Clin. Neurophysiol. 122, 1908–1923. doi:10.1016/j.clinph.2011.05.023, Available at.

Peterson, N.N., Schroeder, C.E., Arezzo, J.C., 1995. Neural generators of early cortical somatosensory evoked potentials in the awake monkey. Electroencephalogr. Clin. Neurophysiol. 96, 248–260 Evoked Potentials.

Restuccia, D., Della Marca, G., Valeriani, M., Rubino, M., Scarano, E., Tonali, P., 2004. Brain-stem components of high-frequency somatosensory evoked potentials are modulated by arousal changes: nasopharyngeal recordings in healthy humans. Clin. Neurophysiol. 115, 1392–1398.

Restuccia, D., Mauguière, F., 1991. The contribution of median nerve SEPs in the functional assessment of the cervical spinal cord in syringomyelia. a study of 24 patients. Brain 114 (Pt 1), 361–379.

Scheer, H.J., Sander, T., Trahms, L., 2006. The influence of amplifier, interface and biological noise on signal quality in high-resolution EEG recordings. Physiol. Meas. 27, 109–117.

Seki, K., Perlmutter, S.I., Fetz, E.E., 2003. Sensory input to primate spinal cord is presynaptically inhibited during voluntary movement. Nat. Neurosci. 6, 1309–1316. Available at http://www.ncbi.nlm.nih.gov/pubmed/14625555. [Accessed September 26, 2013].

Sprenger, C., Eippert, F., Finsterbusch, J., Bingel, U., Rose, M., Büchel, C., 2012. Attention modulates spinal cord responses to pain. Curr. Biol. 22, 1019–1022.

Telenczuk, B., Baker, S.N., Herz, A.V.M., Curio, G., 2011. High-frequency EEG covaries with spike burst patterns detected in cortical neurons. J. Neurophysiol. 105, 2951–2959.

Telenczuk, B., Destexhe, A., 2014. Local field potential, relationship to unit acticity. Encycl. Comput. Neurosci. 1–6. https://scholar.google.de/scholar?hl=de&as_sdt=0%2C5&q=Local+Field+Potential%2C+Relationship+to+Unit+Acticity+telenczuk&btnG=.

Van Diepen, R.M., Mazaheri, A., 2018. The caveats of observing inter-trial phase-coherence in cognitive neuroscience. Sci. Rep. 8, 1–9. doi:10.1038/s41598-018-20423-z, Available at.

Van Wijk, B.C.M., Beek, P.J., Daffertshofer, A., 2012. Neural synchrony within the motor system: what have we learned so far? Front. Hum. Neurosci. 6, 252. Available at http://www.pubmedcentral.nih.gov/articlerender.fcgi?artid=3432872&tool=pmcentrez&rendertype=abstract. [Accessed September 17, 2013].

Ward, L.M., 2003. Synchronous neural oscillations and cognitive processes. Trends Cogn. Sci. 7, 553–559.

Waterstraat, G., Fedele, T., Burghoff, M., Scheer, H.J., Curio, G., 2015. Recording human cortical population spikes non-invasively-an EEG tutorial. J. Neurosci. Methods 250, 74–84. doi:10.1016/j.jneumeth.2014.08.013, Available at.

Waterstraat, G., Körber, R., Storm, J.H., Curio, G., 2021. Noninvasive neuromagnetic single-trial analysis of human neocortical population spikes. Proc. Natl. Acad. Sci. U. S. A. 118.

Waterstraat, G., Telenczuk, B., Burghoff, M., Fedele, T., Scheer, H.J., Curio, G., 2012. Are high-frequency (600Hz) oscillations in human somatosensory evoked potentials due to phase-resetting phenomena? Clin. Neurophysiol. 123, 2064–2073. doi:10.1016/j.clinph.2012.03.013, Available at.

Wikström, H., Huttunen, J., Korvenoja, A., Virtanen, J., Salonen, O., Aronen, H., Ilmoniemi, R.J., 1996. Effects of interstimulus interval on somatosensory evoked magnetic fields (SEFs): a hypothesis concerning SEF generation at the primary sensorimotor cortex. Electroencephalogr. Clin. Neurophysiol. 100, 479–487 Evoked Potentials.

Yamada, T., Kameyama, S., Fuchigami, Y., Nakazumi, Y., Dickins, Q.S., Kimura, J., 1988. Changes of short latency somatosensory evoked potential in sleep. Electroencephalogr. Clin. Neurophysiol. 70, 126–136.

JASP Team (2019) JASP (Version 0.11.1), https://jasp-stats.org/faq/how-do-i-cite-jasp/.